EFDA–JET–PR(13)48

I. Voitsekhovitch, P. Belo, J. Citrin, E. Fable, J. Ferreira, J. Garcia, L. Garzotti,
J. Hobirk, G.M.D. Hogeweij, E. Joffrin, F. Köchl, X. Litaudon, S. Moradi,
F. Nabais, the EU-ITM ITER Scenario Modelling group
and JET-EFDA contributors

# Modelling of JET Hybrid Scenarios with GLF23 Transport Model: E×B Shear Stabilization of Anomalous Transport

“This document is intended for publication in the open literature. It is made available on the understanding that it may not be further circulated and extracts or references may not be published prior to publication of the original when applicable, or without the consent of the Publications Officer, EFDA, Culham Science Centre, Abingdon, Oxon, OX14 3DB, UK.”

“Enquiries about Copyright and reproduction should be addressed to the Publications Officer, EFDA, Culham Science Centre, Abingdon, Oxon, OX14 3DB, UK.”

The contents of this preprint and all other JET EFDA Preprints and Conference Papers are available to view online free at www.iop.org/Jet. This site has full search facilities and e-mail alert options. The diagrams contained within the PDFs on this site are hyperlinked from the year 1996 onwards.

# Modelling of JET Hybrid Scenarios with GLF23 Transport Model: E×B Shear Stabilization of Anomalous Transport

I. Voitsekhovitch[1], P. Belo[2], J. Citrin[3,5], E. Fable[4], J. Ferreira[2], J. Garcia[5], L. Garzotti[1], J. Hobirk[4], G.M.D. Hogeweij[3], E. Joffrin[5], F. Köchl[6], X. Litaudon[5], S. Moradi[7], F. Nabais[2], the EU-ITM ITER Scenario Modelling group and JET-EFDA contributors*

***JET-EFDA, Culham Science Centre, OX14 3DB, Abingdon, UK***

[1]*EURATOM-CCFE Fusion Association, Culham Science Centre, OX14 3DB, Abingdon, OXON, UK*
[2]*Associação EURATOM/IST, Instituto de Plasmas e Fusão Nuclear – Instituto Superior Técnico, Universidade de Lisboa, 1049-001 Lisboa, Portugal*
[3]*FOM Institute DIFFER - Dutch Institute for Fundamental Energy Research, Association EURATOM/FOM, The Netherlands*
[4]*Max-Planck-Institut für Plasmaphysik, EURATOM-IPP Association, Germany*
[5]*CEA, IRFM, F-13108 Saint-Paul-lez-Durance, France*
[6]*Association EURATOM-ÖAW/ATI, Atominstitut, TU Wien, 1020 Vienna, Austria*
[7]*Laboratoire de Physique des Plasmas, Ecole Polytechnique, 91128 Palaiseau, France*
** See annex of F. Romanelli et al, "Overview of JET Results", (24th IAEA Fusion Energy Conference, San Diego, USA (2012)).*

Preprint of Paper to be submitted for publication in
Nuclear Fusion

## ABSTRACT

The $E \times B$ shear stabilisation of anomalous transport in JET hybrid discharges is studied via self-consistent predictive modelling of electron and ion temperature, ion density and toroidal rotation velocity performed with the GLF23 model. The $E \times B$ shear stabilisation factor (parameter $\alpha_E$ in the GLF23 model) is adjusted to predict accurately the four simulated quantities under different experimental conditions, and the uncertainty in $\alpha_E$ determined by 15% deviation between simulated and measured quantities is estimated. A correlation of $\alpha_E$ with toroidal rotation velocity and $E \times B$ shearing rate is found in the low density plasmas, suggesting that the turbulence quench rule may be more complicated than assumed in the GLF23 model with constant $\alpha_E$. For the selected discharges the best predictive accuracy is obtained by using weak/no $E \times B$ shear stabilisation (i.e. $\alpha_E \approx 0$) at low toroidal angular frequency ($\Omega$ < 60krad/s), even in the scenarios with the current overshoot, and $\alpha_E = 0.9$ at high frequency ($\Omega$ > 100krad/s). Interestingly, a weak $E \times B$ shear stabilisation of anomalous transport is found in the medium density strongly rotating discharge. An importance of linear $\beta_e$ stabilisation in this discharge is estimated and compared to the low density discharge with equally high $\beta_e$. The toroidal rotation velocity is well predicted here by assuming that the momentum diffusion coefficient is a fraction of thermal ion diffusivity. Taking into account the $\alpha_E$ and Prandtl number with their uncertainties determined in the modelling of JET hybrid discharges, the performance of ITER hybrid scenario with optimised heat mix (33MW of NBI and 20MW of ECCD) is estimated showing the importance of toroidal rotation for achieving Q > 5.

## 1. INTRODUCTION

The gyro-Landau-fluid (GLF23) model [**1, 2**] is one of the theory-based transport models successfully validated in the modelling of temperature and density evolution in L-mode and H-mode plasmas, hybrid discharges and high $\beta_N$ scenarios on various tokamaks [**3 - 7**]. Although less sophisticated than the trapped gyro-Landau-fluid (TGLF) transport model [**8, 9**] the GLF23 model provides a reasonable compromise between the physics complexity (the main features of the Ion Temperature Gradient (ITG), Trapped Electron Mode (TEM), electron temperature gradient (ETG) turbulence driven transport is captured) and computational time needed for the scenario development and optimisation. The latter requirement is particularly important for the development of the long-pulse operational scenarios in future experiments (for example in ITER) and test of plasma control algorithms. For this reason, further validation of the GLF23 model on existing experimental scenarios is desirable.

The GLF23 model is tested here in simulations performed for seven JET hybrid discharges proposed to the ITER Scenario Modelling (ISM) group for model validation. These discharges have been performed under different experimental conditions (different magnetic field, plasma current and shape, electron density and heating power) by using the current overshoot technique, i.e. the fast current ramp up with its subsequent reduction before the main heating phase [**10**]. Following the current overshoot a broad central region with a relatively flat safety factor $q$ close to one has been formed in these discharges. As a result, MHD stable plasma performance with improved confinement ($H_{98(y,2)}$ increases up to 1.37) has been achieved.

Various physics mechanisms including the reduction of anomalous transport at low magnetic shear and safety factor [**11**], increase of the ITG threshold at high $s/q$ at the outer region of plasma [**7**], stabilising effects of $\beta_e$ [**11**] and the $E\times B$ rotation shear [**5, 11**], fast ion pressure [**12**], improved pedestal confinement [**13**] and neoclassical tearing mode (NTM) stabilisation have been proposed to explain the improved confinement in hybrid scenarios on different tokamaks. The confinement improvement due to stabilisation of the micro-turbulence driven transport has been tested in predictive modelling using the theory-based models (GLF23, TGLF and Weiland models). Focusing here on the stabilising effect of the $E\times B$ velocity shear on the anomalous transport it should be mentioned that in some experiments this effect plays a key role in the confinement improvement while it is less important in others. Thus, the $E\times B$ shear (largely determined by toroidal rotation velocity) contributes significantly to the energy confinement improvement in DIII-D hybrid scenarios as has been shown via predictive modelling with the TGLF transport model [**11**]. However, the modelling of ASDEX Upgrade hybrid [**7**] and improved H-mode discharges [**13**] with the GLF23 and Weiland models shows a relatively weak stabilising effect of the $E\times B$ shear in these plasmas.

The analysis of the $E\times B$ shear stabilisation of anomalous transport (as included in the GLF23 model) in JET hybrid scenarios performed in a broad parameter range is an objective of this study. The $E\times B$ shearing rate is taken into account in the GLF23 model via the reduction of the maximum growth rate with the $E\times B$ shearing as $\gamma_{net} = \gamma_{max} - \alpha_E \gamma_{E\times B}$ (here $\gamma_{max}$ is the maximum growth rate of the drift-ballooning modes in the absence of rotational shear, $\gamma_{E\times B} = (r/q)d(qV_{E\times B}/r)/dr$ is the $E\times B$ shearing rate), with a constant coefficient $\alpha_E$ chosen through fitting to nonlinear gyrofluid simulations. Originally, a broad range of $\alpha_E$ has been suggested ($0.5 < \alpha_E < 1.5$), with a possible dependence of $\alpha_E$ on plasma parameters [**1**].

The turbulence quench rule has been investigated later on in the gyrofluid and gyrokinetic simulations [see for example **14 - 16**]. The early gyrofluid simulations suggested $\alpha_E \approx 1$ over a substantial range of parameters [**14, 15].** The more recent gyrokinetic simulations performed with the GYRO code showed that the turbulence stabilisation can be achieved at different $\alpha_E$ values depending on the parallel velocity shear and density gradient [**16**]. When the parallel velocity shear is neglected, the electron and ion transport is quenched at $\alpha_E \approx 0.5$ for selected plasma parameters, or even at a slightly lower value in plasma with peaked density profile. However, the suppression of anomalous transport requires larger $E\times B$ shear term (or larger $\alpha_E$) in simulations where the destabilizing effect of parallel velocity shear is taken into account [**16**]. At large parallel velocity gradient (PVG) the anomalous transport may not be completely quenched by any level of $E\times B$ shear due to Kelvin-Helmholtz instability leading to faster rise of $\gamma_{max}$ as compared to $\gamma_{E\times B}$. The existence of a broad parameter space where the flow shear is large enough to stabilise the ITG turbulence, but not sufficient for achieving the PVG-dominant regime has been also demonstrated in simulations with GS2 code [**17, 18**]

Attempts were made to validate the $E\times B$ shear stabilisation factor in the GLF23 model for hybrid, high $\beta_N$ and Internal Transport Barrier (ITB) plasmas of DIII-D, AUG and JET where the $E\times B$ shear effect on turbulent transport is expected to be important. The temperatures and density in the regimes with ITB were satisfactory predicted with $\alpha_E = 1.35$ at DIII-D although a high sensitivity to $\alpha_E$ value was reported [**4**]. The evolution of thermal ion ITB starting with its triggering and ending with its degradation was not accurately reproduced with $\alpha_E = 1$ in the ASDEX Upgrade discharge, although the ion temperature was well predicted transiently [**19**]. The modelling of electron and ion temperature in the high $\beta_N$ scenarios of JET performed in a broad parameter space shows a good agreement with measurements obtained with $\alpha_E = 1$ [**6**].
The JET hybrid discharges with different toroidal rotation velocity (and different $E\times B$ shear) are used here to estimate the $E\times B$ shear stabilising effect as included in the GLF23 model addressing in particular to the following questions: (i) would it be possible to predict the plasma profiles using the same fixed $\alpha_E$ value for all selected discharges and (ii) is there any correlation between $\alpha_E$ and plasma parameters in case if the tuning of $\alpha_E$ is needed for each simulated discharge. Such tuning would indicate that important physics mechanisms, responsible for the reduction of anomalous transport in selected hybrid scenarios, may still be missing in the GLF23 model. Based on the correlation of $\alpha_E$ with plasma parameters (if such correlation will be found) a way to extrapolate the GLF23 model to future experiments can be proposed. The peculiarity of the modeling performed here is the self-consistent simulations of electron ($T_e$) and ion ($T_i$) temperature, density of main ion species ($n_i$) and toroidal rotation velocity ($V_{tor}$) (four-field modelling). Such simulations were done for six low density discharges (volume averaged density $\langle n_e \rangle = (2.5–3.4)\times10^{19}$ m$^{-3}$) and one medium density discharge ($\langle n_e \rangle = 4.77\times10^{19}$ m$^{-3}$). Summarising briefly the modelling results for the low density plasmas, it is found that the most accurate prediction of all four simulated quantities is achieved by assuming a correlation of $\alpha_E$ with toroidal rotation velocity or Mach number $M$, with a larger $\alpha_E$ at higher $V_{tor}$ and $M$. In discharges with strong $E\times B$ shear stabilisation the best agreement between the measured and simulated quantities was achieved with $\alpha_E = 0.9$ and $Pr = 0.3$ (the toroidal rotation velocity has been predicted by using $\chi_\varphi = Pr\chi_i$ where $\chi_\varphi$ and $\chi_i$ are momentum and thermal ion diffusivities correspondingly, $Pr$ stands for Prandtl number) determined with a relatively small uncertainties due to strong coupling between the toroidal rotation, temperature and density obtained in simulations with the GLF23 model. In the low density discharges with low rotation and weaker $E\times B$ shear stabilisation $\alpha_E$ reduces to zero and the uncertainty in Prandtl number is relatively large. Interestingly, the stabilising effect of the $E\times B$ shear is found to be weak in the medium density discharge where the toroidal rotation velocity is still large. The effect of the $\beta_e$ stabilisation which could potentially explain the confinement improvement in this and other discharges is discussed, and its impact on the $\alpha_E$ values obtained in discharges with large $\beta_e$ is estimated. Using the $\alpha_E$ and Prandtl number determined in the modelling of JET hybrid discharges the fusion performance of ITER hybrid scenario with optimised heat mix [**20**] is assessed.

This paper is organised as follows. The experimental scenarios and parameter range of simulated hybrid discharges are described in section II. The modelling assumptions and statistical characteristics used here for the estimation of predictive accuracy of the GLF23 models are given in section III. The effect of the $E \times B$ shear on the anomalous transport as included in the electrostatic GLF23 model is estimated in Section IV for seven JET discharges. The $\beta_e$ stabilisation is discussed in Section V which includes the estimation of $\alpha_E$ performed with the electromagnetic GLF23 model for two strongly rotating discharges with the highest $\beta_e$. The four-field modelling of the steady state phase of ITER hybrid scenario with $\alpha_E$ and Prandtl number validated on JET hybrid discharges is presented in section VI. The results are summarised in Section VII.

## 2. EXPERIMENTAL SCENARIOS AND PARAMETER SPACE

Seven JET hybrid discharges where the current overshoot technique [**10**] has been applied are selected for the study of the $E \times B$ shear effect on the anomalous transport (table 1). Four low triangularity ($\delta$) discharges were performed at the same magnetic field $B_t$ plasma current $I_{pl}$ and similar electron density $n_e$, but different neutral beam injection (NBI) power $P_{NBI}$, which was the only auxiliary heating in all selected discharges. The largest achieved $H_{98(y,2)}$ factor varies between 1 and 1.37 in different discharges. Three high triangularity discharges (the last three discharges in table 1) have been performed at different magnetic field, plasma current, electron density and NBI heating power. The toroidal angular frequency and normalised $\beta$ vary strongly over the selected database ($\Omega$ = 79–137krad/s in the plasma centre and $\beta_N$ = 1.66–3.07). A high $\beta_N$ has been achieved under different experimental conditions including a moderate NBI heating at a relatively low plasma current (Pulse No: 75590, $\beta_N = 2.82$) and high NBI heating in plasmas with different shape. In the latter case, close $\beta_N$ values were obtained due to either high density (Pulse No: 77922, $\beta_N = 2.74$) or high temperature (Pulse No: 75225, $\beta_N = 3.07$).

An improved confinement with $H_{98(y,2)} > 1$ (when achieved) was observed during the NBI heating phase following the current overshoot. A half-second time window with the highest $H_{98(y,2)}$ factor and nearly stationary temperature and density has been selected for the analysis and comparison with the modelling results. No or infrequent sawtooth oscillations were observed during this time interval. Four discharges (Pulse No: 75225 and three high triangularity pulses) do not show any NTM activity during the selected time window while weak NTM modes were observed in three other hybrid discharges.

The following diagnostics for the profile measurements have been used here for the comparison with the modelling results. The electron density has been measured using a high resolution Thomson scattering system (HRTS, a spatial resolution of about 1.7cm and time resolution of 50 ms) and cross-validated against the interferometer measurements in simulations performed with the TRANSP code [**21**]. In these simulations the density profiles measured with the HRTS diagnostic have been used as an input and the line integrated density along the interferometer lines of sight has been computed. The HRTS and Electron Cyclotron Emission (ECE, a spatial resolution of about 5 cm and time resolution of 22 ms) diagnostics have been used for electron temperature measurements.

The carbon impurity density, temperature and toroidal rotation velocity have been measured using a 12 channel charge-exchange (CX) diagnostic with a 10ms time resolution, while the deuterium temperature and toroidal rotation velocity have been computed by TRANSP using these data. The safety factor profile has been reconstructed in the EFIT [**22**] simulations using the motional Stark effect (MSE) data as well as the pressure, interferometry and Faraday rotation constraints.

## 3. PLASMA MODEL AND STATISTICAL CHARACTERISTICS FOR PREDICTION ACCURACY

The modelling of electron and ion temperature, ion density and toroidal rotation velocity for selected hybrid scenarios has been performed with the ASTRA code [**23**] using the GLF23 transport model and NCLASS [**24**] for the anomalous and neoclassical transport correspondingly. The NBI heat, particle and momentum sources have been simulated with NUBEAM [**25**] module in TRANSP and used as an input in the ASTRA simulations. Prescribed $q$-profile (EFIT) and $Z_{eff}$ (CX measurements) have been used. The deuterium density has been calculated from the quasi-neutrality equation by TRANSP assuming that carbon is the only impurity. The $E \times B$ shearing rate has been estimated using the self-consistently simulated (or computed by TRANSP in some cases discussed in the next section) deuterium toroidal rotation velocity, density and temperature and neoclassical poloidal rotation velocity. The time-evolving simulations have been performed for the whole NBI heating phase, but only the half-second time window where the largest $H_{98(y,2)}$ factor was achieved has been used for the comparison of experimental and modelling results.

While the NBI deuterium particle source is estimated with some level of confidence (the fast ion energy computed by TRANSP is validated by comparing the diamagnetic energy calculated by EFIT and TRANSP) an accurate estimation of the deuterium source coming from the gas puff and recycling is a challenging problem. In this work the influx of puffed and recycled deuterium neutrals through the separatrix is estimated in the self-consistent core-pedestal-SOL simulations using the TRANSP and EDGE2D [**26**] codes iteratively. First, the thermal electron and ion fluxes through the separatrix to SOL as well as the ion particle flux produced by NBI have been calculated by TRANSP and used as an input to EDGE2D code which performs the simulations of electron and ion temperature and density in the pedestal and SOL regions. The transport coefficients in the pedestal region have been carefully tuned in the EDGE2D simulations for obtaining an accurate prediction of measured electron density and temperature profiles as well as the outermost $T_i$ value. Then, the deuterium neutral influx through the separatrix calculated by EDGE2D has been used by TRANSP for the estimation of neutral penetration, ionisation and charge exchange as well as the NBI charge exchange losses. The neutral simulations in TRANSP have been performed with the FRANTIC module [**27**]. The thermal and NBI deuterium particle fluxes to SOL estimated in these TRANSP simulations have been used as an input to EDGE2D. The TRANSP - EDGE2D simulations of the low (6 MW, Pulse No: 79635) and high (17 MW, Pulse No: 77922) power discharges show that the neutral influx in these discharges is in the range $(3.3–3.5)\times 10^{21}$ part/s. Similar neutral influx has been assumed in the FRANTIC/TRANSP simulations of other discharges.

The modelling of electron and ion temperature, density and toroidal rotation velocity has been performed in the plasma region 0 ≤ ρ ≤ 0.8–0.85, with the outer boundary determined by the location of the outmost CX data point (ρ is a square root of normalised toroidal flux). The predictive accuracy of the GLF23 model was estimated in the radial region 0.25 < ρ < 0.65 (i. e. excluding the plasma centre where the drift modes are likely to be stable and the region near the simulation boundary) using the standard expressions for the root-mean-square (rms) deviation and

$$rms = \left[ \frac{1}{NL} \sum_{t_n = t_1}^{t_N} \sum_{\rho_l = 0.25}^{\rho_l = 0.65} \frac{\left\{ X_{\exp}(t_n, \rho_l) - X_{sim}(t_n, \rho_l) \right\}^2}{X_{\exp}(t_n, \rho_l)^2} \right]^{1/2}$$

$$offset = \frac{1}{NL} \sum_{t_n = t_1}^{t_N} \sum_{\rho_l = 0.25}^{\rho_l = 0.65} \frac{X_{\exp}(t_n, \rho_l) - X_{sim}(t_n, \rho_l)}{X_{\exp}(t_n, \rho_l)}$$

Here $t_1$ and $t_N$ are the start and the end of selected time window (0.5 s) with $N$ time slices, $X_{exp}$ and $X_{sim}$ stand for the experimental and simulated quantities respectively (i.e. $T_i$, $T_e$, $n_i$ and $V_{tor}$) and $L$ is a number of radial points in the interval 0.25 < ρ < 0.65.

## 4. *E*×*B* SHEAR SUPPRESSION OF ANOMALOUS TRANSPORT IN SIMULATIONS WITH ELECTROSTATIC GLF23 MODEL

Three different sets of simulations have been performed to test the importance of the four-field ($T_e$, $T_i$, $n_i$ and $V_{tor}$) coupling in the GLF23 model and the *E*×*B* shear stabilisation under various experimental conditions. The *E*×*B* shear stabilisation factor $\alpha_E$ has been varied from zero to 1.3 within each set of simulations for each simulated discharge.

First, the coupled simulations of electron and ion temperature have been performed using the prescribed density of all plasma species and toroidal rotation velocity. The rms deviation and offset for $T_e$ and $T_i$ obtained in these simulations are shown on Fig.1 for four different $\alpha_E$ values. The discharges on Fig.1 are arranged in the order of increasing toroidal angular frequency, which is indicated on the horizontal axis (similar arrangement is used on Figs.2 and 3). This angular frequency is estimated at the inner boundary of the region where the drift modes are still unstable (at ρ = 0.25). When the *E*×*B* shear stabilisation is neglected (left columns for each discharge obtained with $\alpha_E$ = 0) the temperatures are under-predicted in all discharges, with a particularly large deviation from the measurements (up to 30%) in the low density discharges with the largest toroidal rotation. The prediction accuracy is slightly better at low NBI power and toroidal rotation velocity (Pulse No's: 79635 and 74641) and in the medium density Pulse No: 77922. The temperature prediction improves in all discharges with an increase of $\alpha_E$. The best agreement with measurements is achieved with $\alpha_E$ = 1 in the low density discharges Pulse No's: 79635, 74641, 74634, 75590 and 74637 while a larger $\alpha_E$ is needed for an accurate temperature prediction in the discharge with largest $V_{tor}$ (Pulse No: 75225, $\alpha_E$ = 1.3). In the medium density discharge the temperatures are well predicted at a lower $\alpha_E$ ($\alpha_E$ = 0.5) showing that the $E\times B$ shear stabilisation plays less important role in the suppression of the core anomalous transport in this discharge.

As a next step, the statistical estimation of the GLF23 predictive accuracy has been performed in the three-field simulations ($T_e$, $T_i$ and $n_i$) using the measured toroidal rotation velocity (Fig.2). Although a qualitatively similar change of predictive accuracy with an increase of $\alpha_E$ has been obtained in all discharges, the $\alpha_E$ values providing the most accurate prediction are different in the two-field and three-field simulations. At low density the best agreement between the simulations and measurements (estimated as a largest deviation from the measurements over all three simulated quantities) is obtained with $\alpha_E$ = 0.5 in the weakly rotating discharges Pulse No's: 79635 and 74641 while the larger $\alpha_E$ values are needed to predict accurately the temperature and density at high toroidal rotation. As in the previous set of simulations, a better agreements with the GLF23 computed plasma profiles is obtained with $\alpha_E$ = 0.5 in the medium density discharge where the $E\times B$ shear stabilisation appeared to be as weak as in the low density discharges with low toroidal rotation velocity.

By comparing the effect of the $E\times B$ shear on thermal and particle transport in the low density discharges with $\Omega$ > 80 krad/s (where the $E\times B$ shear is expected to produce a visible stabilising effect) one can see that the best density prediction is obtained with $\alpha_E$ = 0.5 while the ion temperature is well predicted with $\alpha_E$ = 1.3 (Pulse No's: 775590, 74637 and 75225). Indeed, these discharges have a relatively weak density peaking as compared to the ion temperature peaking which can be better predicted with low $\alpha_E$. This observation shows that a compromise in the choice of $\alpha_E$ should be made for high rotation discharges to predict the ion temperatures and density equally well in the three-field simulations. In contrary, the ion temperature and density can be well predicted with nearly the same $\alpha_E$ values in discharges with weak $E\times B$ shear stabilisation.

The last set of simulations includes the modelling of electron and ion temperature, deuterium density and toroidal rotation velocity. It should be mentioned that the four-field coupling is important in simulations with the GLF23-computed transport, in particular for the prediction of the toroidal rotation velocity. The toroidal rotation velocity is strongly over-estimated in the simulations with fixed $T_e$, $T_i$ and $n_i$ in JET hybrid discharges due to the self-driven $E\times B$ shear stabilisation increasing with $V_{tor}$. In the coupled four-field simulations the temperature and density gradients, increasing with rotation and driving the anomalous transport, restrict the runway of toroidal rotation velocity. In present simulations the momentum diffusivity $\chi_\varphi$ includes the GLF23-computed and neoclassical terms, with the neoclassical diffusivity $\chi_{\varphi,neocl}$ = (0.3 - 1)$\chi_{i,neocl}$ ($\chi_{i,neocl}$ is thermal ion neoclassical diffusivity computed with NCLASS). The ratio $\chi_{\varphi,neocl}/\chi_{i,neocl}$ was adjusted to match the measured toroidal rotation velocity near the plasma centre where the GLF23-computed transport is generally stable. Two options for the anomalous momentum diffusivity have been tested here. First, the four-field simulations have been performed with the GLF23 computed momentum diffusivity and $\alpha_E$ value providing the best agreement for temperatures and densities (as determined in the three-field simulations, Fig.2). The toroidal rotation velocity has been strongly overestimated in these simulations (by 25–80%). Second, the anomalous momentum diffusivity was assumed to be a fraction of the anomalous thermal ion diffusivity ($\chi_\varphi = Pr\chi_i$) computed with the GLF23 model. Different Prandtl numbers have been tested for selected discharges. With $Pr = 1$, a strongly underestimated toroidal rotation velocity (by factor ~2 - 2.5 even with $\alpha_E = 1.3$) has been obtained for all selected low density discharges. The most accurate prediction of all simulated quantities including $V_{tor}$ in the low density discharges Pulse No's: 74641, 74634, 75590, 74637 and 75225 has been achieved by using $Pr = 0.3$ (the rms deviation is less than 18%). The modelling of all selected discharges performed with $Pr = 0.3$ and different $\alpha_E$ shows that the $\alpha_E$ value providing the best predictive accuracy increases from 0.5 (Pulse No's: 74641, 74634) to 1 (Pulse No's:75590, 74637 and 75225) with toroidal rotation velocity (Fig.3). In the discharge with the lowest observed toroidal rotation (Pulse No: 79635) and in the medium density discharge Pulse No: 77922 where the $E\times B$ shear stabilisation effect is weak, the toroidal rotation velocity is strongly over-predicted with $Pr = 0.3$, even at zero $\alpha_E$. By increasing the Prandtl number at least to 0.36 in Pulse No:79635 and to 0.4 in Pulse No: 77922 a satisfactory agreement between the simulations and measurements has been achieved for all four quantities (less than 15% rms deviation with $\alpha_E = 0$).

The correlation between $\alpha_E$ and toroidal angular frequency found in the previous simulations is illustrated in figure 4. The results shown in this figure have been obtained by performing a small-step variation of $\alpha_E$ around its value, providing the most accurate agreement between the modelling results and measurements. These values for each discharge are shown by the black circles in figure 4. The vertical lines indicate the range of $\alpha_E$ where the rms deviation and offset are below 15% for any simulated quantity. $Pr = 0.3$ is used for all discharges except Pulse No: 79635 ($Pr = 0.36$) and Pulse No: 77922 where the choice of $Pr$ will be discussed later on. Figure 4 (top) shows a non-linear correlation of the $E\times B$ shear stabilisation with toroidal rotation velocity, with an initial increase of $\alpha_E$ with $V_{tor}$ and subsequent flattening. A large $\alpha_E$ uncertainty has been found in the discharges with low and medium $\Omega$ (Pulse No's: 74641 and 74634), with good prediction (less than 15% deviation from the data), obtained in a relatively wide range of $\alpha_E$. This uncertainty is a consequence of the weak stabilising effect of the $E\times B$ shear in these discharges leading to a weak coupling between the toroidal rotation velocity and other simulated quantities. In contrary, in the discharges with an efficient $E\times B$ shear stabilisation a small variation in toroidal rotation strongly affects $n_i$ and $T_i$ prediction reducing the choice of $\alpha_E$, i.e. all simulated quantities are strongly coupled. In terms of dimensionless parameters a similar correlation of $\alpha_E$ with the Mach number estimated as a ratio of the toroidal rotation velocity to the thermal ion (Fig.4 bottom) or thermal electron velocity has been found.

In selected discharges the $E\times B$ shearing rate $\gamma_{E\times B}$ increases with toroidal rotation velocity suggesting a correlation between $\alpha_E$ and $\gamma_{E\times B}$ (i.e. a non-linear quench rule with respect to $E\times B$ shear). Indeed, some correlation between these two quantities has been found (Fig.5). The $E\times B$ shearing rate used in figure 5 has been estimated with the measured temperatures, density and toroidal rotation velocity. As follows from the analysis of five low density discharges, $\alpha_E$ increases with an increase of shearing rate at low $\gamma_{E\times B}$ and it remains constant (as assumed in the GLF23 model) at high $\gamma_{E\times B}$. The low current discharge with high $\beta_N$ (Pulse No: 75590) and strong $E\times B$ shear stabilisation achieved at a relatively low $\gamma_{E\times B}$ is slightly outside this trend as well as the medium density discharge Pulse No: 77922 with large $\alpha_E$ uncertainty.

The correlation of $\alpha_E$ with the ratio of ion to electron temperature $T_i/T_e$ has been also checked (Fig. 6). The $T_i/T_e$ ratio affects the ITG turbulence threshold which increases as $(1 + T_i/T_e)$ in the flat density limit [**28**]. Indeed, there is a correlation between the suppression of anomalous transport, characterised by $\alpha_E$, and $T_i/T_e$, i.e. the suppression of the anomalous transport is more efficient at larger $T_i/T_e$ ratio (Fig.6). However this correlation may be a consequence of the reduction of the thermal ion transport due to strong $E\times B$ shear which triggers an increase of $T_i$, rather than the illustration of the $T_i/T_e$ effect on the ITG mode threshold.

The uncertainty in $\alpha_E$ and *Pr* estimated in the four-field simulations for discharge Pulse No: 77922 where the $E\times B$ shear stabilisation is found to be weak ($\alpha_E$ = 0.5) in spite of the large toroidal rotation velocity is shown in figure 7. The $\alpha_E$ - *Pr* domain is limited by the 15% deviation between the simulations and measurements applied to the less accurately predicted quantity (Fig. 7, red solid curve). Depending on the choice of *Pr* the uncertainty in $\alpha_E$ varies between zero and 1.05 while the uncertainty in the Prandtl number is between 0.4 and 0.95. Much smaller *Pr* and $\alpha_E$ uncertainties are found in the discharges with strong $E\times B$ shear stabilisation due to the strong coupling between ion temperature, density and toroidal rotation velocity (uncertainty in *Pr* and $\alpha_E$ in Pulse No: 75225 are shown in Fig. 7 for comparison with Pulse No: 77922).

As a final remark, it should be mentioned that the correlation of the $E\times B$ shear strength with plasma rotation or $\gamma_{E\times B}$ in the GLF23-computed turbulence quench rule illustrated in this section may hide other physics effects, not taken into account in the GLF23 model, like for example the nonlinear electromagnetic stabilisation of ITG turbulence, which can also be enhanced by fast ions [**29, 30**]. It is difficult to separate the stabilising effects of fast ion pressure gradient and $E\times B$ shear in the high power JET hybrid discharges where both the toroidal rotation velocity and fast ion pressure increase with power. Further experiments with high NBI power and low injected torque would be useful to clarify the contribution of both effects to the suppression of anomalous transport.

## 5. ESTIMATION OF $E\times B$ SHEAR EFFECT IN PRESENCE OF LINEAR $\beta_E$ STABILISATION

Previous simulations have been performed with electrostatic version of the GLF23 model. To estimate the importance of electromagnetic effects the four-field simulations have been repeated with electromagnetic GLF23 model for two selected discharges, low density and high temperature discharge Pulse No: 75225 and medium density discharge Pulse No: 77922 with lower electron temperature and larger magnetic field. Nearly similar values of electron beta $\beta_e$ have been obtained in these discharges, with its central and mid-radius values equal to 0.02–0.023 and 0.009

respectively. The electromagnetic effects are expected to relax the requirements to the $E \times B$ shear stabilisation allowing a similarly good prediction at lower $\alpha_E$ values as compared to electrostatic GLF23 simulations. Indeed, the $\alpha_E$ value providing the most accurate prediction reduces by 30% in discharge Pulse No: 75225, with a little influence of electromagnetic effects on the choice of Prandtl number. Much larger impact of electromagnetic effects on the choice of $\alpha_E$ and $Pr$ as compared to electrostatic case was obtained in Pulse No: 77922 leading to the reduction of the upper limit of $\alpha_E$ nearly by factor 2. The $Pr$–$\alpha_E$ domain, determined by 15% deviation between the simulations and measurements, is shifted towards larger Prandtl numbers (Fig.7, red dashed curve).

Using the GLF23 model, the influence of electromagnetic effects on the maximum linear growth rate has been tested for the same two discharges by artificially enhancing the $\beta_e$ stabilisation. This has been done in interpretative simulations (i.e. with measured $T_e$, $T_i$, $n_i$ and $V_{tor}$) by changing the multiplier in front of $\beta_e$, $C_{\beta e}$, in the GLF23 model. The artificial $\beta_e$ values used by the GLF23 model in this case $\beta_{e,GLG23} = C_{\beta e}\beta_{e,exp}$ are inconsistent with the measured electron pressure. Figure 8 (top) shows the evolution of the maximum linear growth rate at $\rho = 0.4$, where it is determined by the ITG turbulence. The growth rate reduces with $\beta_e$ during the $C_{\beta e}$ scan in two selected discharges until the MHD dominant domain characterised by large negative frequencies (modes propagating in the ion diamagnetic direction) is reached. The medium density operational point (Pulse No: 77922) appeared to be much closer to the onset of MHD modes than the low density point (Pulse No: 75225) where the transition to MHD-dominant regime occurs at $\beta_e = 0.047$ (not shown in Fig.8). Strong $\beta_e$ stabilisation of the ITG turbulence in discharge Pulse No: 77922 and operation close to the kinetic ballooning mode (KBM) dominant domain has been also found in GYRO simulations [**31, 32**], with the KBM onset at $\beta_e = 0.011$ while the GLF23 estimated MHD onset is around $\beta_e = 0.028$ in this discharge.

The effect of linear $\beta_e$ stabilisation on plasma parameters has been also tested in the self-consistent four-field simulations (Fig.9). Similarly to the previous case the parameter $C_{\beta e}$ has been varied, but $\beta_e$ has been computed for each $C_{\beta e}$ value using predicted electron density and temperature. The modelling has been performed with $\alpha_E$ and $Pr$ which provide a reasonably accurate prediction for four simulated quantities ($\alpha_E = 0.25$, $Pr = 0.9$ in Pulse No: 77922 and $\alpha_E = 0.9$, $Pr = 0.3$ in Pulse No: 75225). The $\beta_e$ stabilisation enhanced by increasing $C_{\beta e}$ from zero (electrostatic case) to 2.5-3 leads to the increase of ion temperature (Fig.9 bottom) and toroidal rotation velocity in two simulated discharges. Electron temperature is weakly affected, slightly increasing with $C_{\beta e}$. Although the $\beta_e$ effects are stabilising the maximum linear growth rate increases with $C_{\beta e}$ due to increased ion temperature until the MHD dominant domain is reached. The volume averaged density reduces with $C_{\beta e}$ in Pulse No: 77922 while it is nearly unchanged at low $C_{\beta e}$ and slightly increases at high $C_{\beta e}$ in Pulse No: 75225 (Fig.9 bottom). Consequently, the $\beta_e$ stabilisation improves the thermal energy content in simulations performed for Pulse No: 75225, where $\beta_e$ increases with $C_{\beta e}$. However, the density reduction with $C_{\beta e}$ in Pulse No: 77922 prevents an increase of $\beta_e$, and thermal energy weakly evolves in this discharge during the $C_{\beta e}$

scan (Fig.9 middle). It should be mentioned that the effect of $\beta_e$ stabilisation, affecting differently the performance in two selected discharges, strongly depends on the choice of $\alpha_E$. The $C_{\beta e}$ scan performed at low $\alpha_E$ in discharge 75225 shows moderate temperature increase and strong density reduction making the $\beta_e$ stabilisation inefficient.

The range of $C_{\beta e}$ values used in Fig.9 is limited by the MHD mode onset reached at $C_{\beta e}$ = 2.5 in Pulse No: 77922 and $C_{\beta e}$ = 3 in Pulse No: 75225. The density increases and temperatures and toroidal rotation velocity reduce with $C_{\beta e}$ in the MHD-dominant domain. The onset of MHD modes obtained in the self-consistent modelling for discharge Pulse No: 77922 occurs at the same $\beta_e$ as the KBM onset in the GYRO simulations of the same discharge. However one should keep in mind that this MHD onset has been estimated by using an enhanced $\beta_e$ (multiplied by $C_{\beta e}$ coefficient) in the GLF23 model rather than actual $\beta_e$, obtained in the self-consistent predictive simulations.

## 6. FOUR-FIELD MODELLING OF ITER HYBRID SCENARIO: EFFECT OF $E\times B$ SHEAR AND $\beta_E$ STABILISATION

Beneficial effects of the $E\times B$ shear and linear $\beta_e$ stabilisation on fusion performance are estimated here for ITER hybrid scenario with optimised heat mix developed within the ISM group [**20**]. Following the results of Ref. **20** the main heating phase of this scenario has been simulated using 33MW of NBI and 37 MW of ECRF heating applied during the 12MA plasma current flat-top. The NBI simulations (heat and particle sources, beam driven current, torque and beam ion density) have been done with the Fokker-Planck NBI module implemented in ASTRA. This module has been successfully benchmarked against NUBEAM [**33**]. The electron cyclotron heating and current density profiles have been taken from the simulations performed in ref. **20**. Current diffusion has been simulated using NCLASS for the bootstrap current and resistivity. Deuterium density has been computed using the deuterium NBI fuelling while tritium density was assumed to be equal to deuterium density. The pedestal density which allows one to keep the GLF23-predicted density profiles close to the Greenwald density limit has been chosen. The pedestal temperature $T_{i,ped}$ = $T_{e,ped}$ = 5 keV has been assumed for the reference case, and the sensitivity to this parameter has been tested. A simplistic assumption of zero toroidal rotation velocity at the pedestal has been used. The simulations with different GLF23 settings have been performed to illustrate the stabilising effects of the $E\times B$ shear and $\beta_e$. First, the simulations with zero toroidal rotation velocity and $\alpha_E$ = 0.5 have been done. A relatively low alpha heating ($P_\alpha$ = 57.5MW) and fusion $Q$ (= 4.2) have been obtained with the electrostatic GLF23 model in this case, with 4% improvement due to electromagnetic effects ($C_{\beta e}$ = 1). Second, the toroidal rotation velocity has been simulated self-consistently with other parameters using the most optimistic GLF23 settings ($\alpha_E$ = 0.9 and $Pr$ = 0.3) validated in simulations of low density and high rotation JET hybrid discharges. The temperature, density and $q$-profiles obtained in the electrostatic simulations performed with and without toroidal rotation velocity are compared in Fig.10. Higher alpha heating ($P_\alpha$ = 79.4MW) than in the non-rotating plasma, and $Q$ = 5.8 have been obtained with simulated toroidal rotation velocity (Fig.10 bottom right). The hybrid-like $q$-profile with minimum $q$ value above one was maintained stationary (Fig.10, bottom left) with the total fraction of non-inductive currents about 50%. The fusion $Q$ increases by 12% in the simulations with electromagnetic GLF23 model due to linear $\beta_e$ stabilisation. The self-consistent four-field simulations repeated with the less optimistic GLF23 settings based on the modelling of the medium density discharge Pulse No: 77922 ($Pr$ = 0.6 and $\alpha_E$ = 0.6) show that the fusion $Q$ reduces from 5.8 to 4.8.

It should be mentioned that a low Mach number and $T_i/T_e$ ratio ($M \approx 0.11$ and $T_i/T_e \approx 1$) have been obtained in the ITER hybrid scenario simulated with the most optimistic GLF23 settings $Pr$ = 0.3 and $\alpha_E$ = 0.9. A projection based on these dimensionless parameters (i.e., towards low Mach number (Fig.4 bottom) or low $T_i/T_e$ ratio (Fig.6)) suggests that $\alpha_E$ should be close to zero in simulations of ITER hybrid scenario resulting in low fusion performance ($Q \approx 4$).

The sensitivity of the most optimistic scenario obtained with $Pr$ = 0.3 and $\alpha_E$ = 0.9 to pedestal temperature has been tested in simulations with electrostatic GLF23 model. Fusion $Q$ reduces below five with the reduction of pedestal temperature to 4.25keV showing that the operation with $Q > 5$ can be achieved within a relatively narrow range of pedestal temperatures for simulated hybrid scenario.

## 7. SUMMARY AND DISCUSSION

The capability of the GLF23 model to predict the thermal, particle and momentum transport by artificially enhancing the $E\times B$ shear stabilisation with an increase of toroidal rotation or Mach number has been demonstrated in the self-consistent simulations of electron and ion temperature, ion density and toroidal rotaion velocity performed for seven JET hybrid discharges. The $E\times B$ shear strength has been varied by changing the multiplier $\alpha_E$ in the quench rule $\gamma_{max} = \alpha_E \gamma_{E\times B}$. The most accurate prediction of four simulated quantities in the low density plasmas with various NBI powers and toroidal rotation velocities has been obtained by varying $\alpha_E$ from zero to 0.9 with an increase of toroidal angular frequency in the range 46–85 krad/s and keeping $\alpha_E$ constant at $\Omega > 85$ krad/s. Similar correlation between $\alpha_E$ and Mach number has been found. These correlations are outside the $\alpha_E$ uncertainties limited here by the 15% rms deviation between predicted quantities and their measurements. The correlation of $\alpha_E$ with other parameters controlling turbulence stabilisation, namely $\gamma_{E\times B}$ and $T_i/T_e$, is less pronounced than its correlation with $V_{tor}$ or $M$. The modelling results presented here suggest that the improvement of quench rule in the GLF23 model would be highly desirable for an accurate prediction of temperatures, density and toroidal rotation velocity in the JET hybrid discharges with different rotation. A new $E\times B$ shear stabilisation paradigm which takes into account a shift in the peak of the radial wave number spectrum of electric potential fluctuations induced by the $E\times B$ velocity Doppler shift as well as the reduction in their amplitude has been recently suggested and implemented in the TGLF transport model [**34, 35**]. The toroidal Reynolds stress, non-linearly dependent on $\gamma_{E\times B}$, has been estimated within this approach improving the prediction for toroidal momentum. A test of the $E\times B$ shear spectral shift model as implemented in TGLF in the simulations of JET hybrid discharges with different toroidal rotation is envisaged in future to clarify the role of the $E\times B$ shear suppression of anomalous transport in these plasmas. It should be mentioned that the application of the $E\times B$ shear quench rule with $\alpha_E$, dependent on plasma parameters, may not be a unique option for predicting accurately the plasma profiles. The non-linear $\beta$ stabilisation of electromagnetic turbulence [**29**] or stabilising effects of fast ion pressure gradient [**30**] could also contribute to the confinement improvement and relax the requirements to $\alpha_E$. Unfortunately, it is not possible to separate the influence of these effects from the $E\times B$ shear stabilisation in selected JET discharges where the fast ion pressure, $\beta$ and $\gamma_{E\times B}$ co-correlate, increasing with NBI power. Since the first two stabilising mechanisms are not implemented in the available theory-based transport models it is impossible to make quantitative estimations of these effects in predictive modelling. The gyrokinetic simulations of discharges analysed here are needed for concluding about the full or partial contributions of other non-linear effects to the core confinement improvement in different plasma regions.

The toroidal rotation velocity has been well predicted in selected discharges using $\chi_\varphi = Pr\chi_i$, and the Prandtl number has been estimated with uncertainties under different experimental conditions. In the strongly rotating low density discharges the toroidal rotation velocity is accurately reproduced with $Pr = 0.3$, with a relatively small uncertainties due to strong coupling between $V_{tor}$ and other simulated quantities via the $E\times B$ shear stabilisation. Under some conditions (dominant ITG turbulence, relatively low density peaking) the thermal and momentum diffusivities are supposed to be similar [**36**], and the Prandtl number below one found here could be considered as an indication of momentum pinch. In plasmas with low $E\times B$ shear stabilisation (Pulse No's: 79635, 74641 and 77922) the toroidal rotation is weakly coupled with the density and temperatures in the self-consistent GLF23-based simulations. As a result, the Prandtl number and $\alpha_E$ are estimated with a much larger uncertainties in these discharges as compared to the strongly rotating plasmas.

The importance of the three-field coupling in the GLF23-based simulations is assessed by comparing the temperature only prediction with the self-consistent simulations of temperatures and density. This comparison shows that the $E\times B$ shear (as included in the GLF23 model) suppresses the thermal transport more efficiently than the particle transport in selected discharges. Based on this result and also on the variation of $\alpha_E$ with toroidal rotation velocity or Mach number (Fig.4), a "compromised" $\alpha_E$ value, fixed for all simulated discharges, has been suggested in Refs. **32** and **37** ($\alpha_E = 0.5$), but the overall predictive accuracy obtained with this $\alpha_E$ is much lower.

The influence of linear $\beta_e$ stabilisation on thermal, particle and momentum transport has been examined by comparing the simulations performed with the electrostatic and electromagnetic GLF23 model for two strongly rotating discharges with different densities and temperatures (Pulse No's: 77922 and 75225), but similar $\beta_e$. Strong reduction of the maximum linear growth rate, driven by the ITG turbulence, with $\beta_e$ has been found in the interpretative simulations with the GLF23 model indicating that $\beta_e$ stabilisation could be important in these discharges. However, the self-consistent simulations taking into account the strong non-linear coupling between temperatures, density and toroidal rotation velocity via GLF23-computed transport and power balance show limited effect of $\beta_e$ on plasma performance when the $E\times B$ shear stabilisation is weak (i.e. at low $\alpha_E$). Although the temperatures and toroidal rotation velocity do increase due to $\beta_e$ stabilisation at low and high $\alpha_E$, the density strongly reduces in simulations with low $\alpha_E$ (Pulse No: 77922) leading to a relatively small increase in thermal energy.

The uncertainty in fusion performance in ITER hybrid scenario with optimised heat mix [**20**] has been estimated taking into account the uncertainties in $\alpha_E$ and *Pr* found in JET hybrid discharges. While a low fusion *Q* has been obtained with zero toroidal rotation velocity ($Q$ = 4.2) the plasma performance has been improved in simulations which include the self-consistent modelling of toroidal rotation velocity, temperatures and density illustrating the importance of toroidal rotation for achieving Q > 5. Further improvement of ITER hybrid performance can be expected from other stabilising effects, such as non-linear $\beta_e$ stabilisation with strong contribution of alpha-particle pressure.

**ACKNOWLEDGEMENTS**
Dr. C. Angioni is warmly acknowledged for useful discussions. We would like to thank Drs. M. Brix and N. Hawkes for their help in reconstructing the *q* profiles for discharges used in this paper. This work was carried out within the framework of the Task Force on Integrated Tokamak Modelling of the European Fusion Development Agreement. The views and opinions expressed herein do not necessarily reflect those of the European Commission. This work was also part-funded by the RCUK Energy Programme under grant EP/I501045.

**REFERENCES**

[1]. R.E. Waltz, G.M. Staebler, W. Dorland et al, Physics of Plasmas **4** (1997) 2482
[2]. R.E. Waltz and R.L. Miller, Physics of Plasmas **6** (1999) 4265
[3]. C.C. Petty, J.E. Kinsey and T.C. Luce, Physics of Plasmas **11** (2004) 1011
[4]. J.E. Kinsey, G.M. Staebler and R.E. Waltz, Physics of Plasmas **12** (2005) 052503
[5]. P.A. Politzer, C.C. Petty, R.J. Jayakumar et al, Nuclear Fusion, **48** (2008) 075001
[6]. I. Voitsekhovitch, B. Alper, M. Brix et al, Nuclear Fusion **49** (2009) 055026
[7]. J. Citrin, J Hobirk, M Schneider et al, Plasma Physics and Controlled Fusion, **54** (2012) 065008
[8]. G.M. Staebler, J.E. Kinsey, R.E. Waltz, Physics of Plasmas **14** (2007) 055909
[9]. G.M. Staebler and J.E. Kinsey, Physics of Plasmas **17** (2010) 122309
[10]. J. Hobirk, F. Imbeaux, F. Crisanti et al, Plasma Physics and Controlled Fusion **54** (2012) 095001
[11]. J.E. Kinsey, G.M. Staebler, and C.C. Petty, Physics of Plasmas **17** (2010) 122315
[12]. J. Garcia, N. Hayashi, B. Baiocchi et al, "Physics comparison and modelling of the JET and JT-60U core and edge:towards JT-60SA predictions", 14$^{th}$ International Workshop on H-mode physics and Transport Barriers, Fukuoka, Japan, October 2-4 2013

[13]. Y.-S. Na, G.D. Conway, O. Gruber, et al, Nuclear Fusion **46** (2006) 232
[14]. R.E. Waltz, G.D. Kerbel and J. Milovich, Physics of Plasmas **1** (1994) 2229
[15]. R.E. Waltz, R.L. Dewar and X. Garbet, Physics of Plasmas **5** (1998) 1784
[16]. J.E. Kinsey, R.E. Waltz and J. Candy, Physics of Plasmas **12** (2005) 062302
[17]. E.G. Highcock, M. Barnes, A.A. Schekochihin et al, Physical Review Letters **105** (2010) 215003
[18]. F.I. Parra, M. Barnes, E.G. Highcock et al, Physical Review Letters **106** (2011) 115004
[19]. G. Tardini, J. Hobirk, V.G. Igochine et al, Nuclear Fusion **47** (2007) 280
[20]. J. Citrin, J. F. Artaud, J. Garcia et al, Nuclear Fusion **50** (2010) 115007
[21]. R.J. Goldston, D.C. McCune, H.H. Towner et al, Journal of Computational Physics **43** (1981) 61
[22]. D.P. O'Brien et al Nuclear Fusion **32** (1992) 1351
[23]. G.V. Pereverzev and P.N. Yushmanov 2002 Report IPP 5/98, Max-Planck-Institute fur Plasmaphysik
[24]. W.A. Houlberg, K.C. Shaing, S.P. Hirshman and M.C. Zarnstorff, Physics of Plasmas **4** (1997) 3230
[25]. A. Pankin, D. McCune, R. Andre et al, Computer Physics Communications **159** (2004) 157
[26]. R. Simonini, G. Corrigan et al, Computer Physics Communications **34** 2/3 (1994) 368
[27]. A.A. Korotkov and A.N. Zinov'ev, Soviet Journal of Plasma Physics **15** (1989) 136
[28]. S.C. Guo and F. Romanelli, Physics of Fluids **B5** (1993) 520
[29]. M.J. Pueschel and F. Jenko, Physics of Plasmas **17** (2010) 062307
[30]. J. Citrin, F. Jenko, P. Mantica et al, Physical Review Letters **111** (2013) 155001
[31]. S. Moradi, I. Pusztai, I. Voitsekhovitch et al, to be submitted to Nuclear Fusion
[32]. I. Voitsekhovitch, X. Litaudon, E. Barbato et al, 39$^{th}$ EPS Conference on Plasma Phys., Stockholm, 2-6 July 2012, P4-066
[33]. M. Fitzgerald, I. Voitsekhovitch, H. Leggate et al, 33$^{rd}$ EPS Conference on Plasma Phys., Rome, 19 - 23 June 2006, ECA Vol. 30I, P-1.079 (2006)
[34]. G.M. Staebler, R.E. Waltz, and J.E. Kinsey, Physics of Plasmas **18** (2011) 056106
[35]. G.M. Staebler, R.E. Waltz, J. Candy, and J.E. Kinsey, Physical Review Letters **110**, 055003 (2013)
[36]. N. Mattor and P. H. Diamond, Physics of Fluids **31** (1988) 1180
[37]. X. Litaudon, I. Voitsekhovitch, J.F. Artaud et al, Nuclear Fusion **53** (2013) 073024

| Pulse # | $B_t$, T | $I_{pl}$ MA | $P_{NBI}$ MW | $n_l$ / $10^{19}$ $m^{-3}$ | Ω at 3 m, krad/s | $H_{98(y,2)}$ | P(ρ=0.8), kPa | $\beta_N$ |
|---|---|---|---|---|---|---|---|---|
| 74641 | 2 | 1.7 | 9.3 | 3.4 | 79 | 1 | 9 | 1.66 |
| 74634 | 2 | 1.7 | 17.5 | 3.4 | 95 | 1.05 | 13 | 2.47 |
| 74637 | 2 | 1.7 | 18.9 | 3.2 | 137 | 1.17 | 12 | 2.81 |
| 75225 | 2 | 1.7 | 18 | 3.2 | 127 | 1.35 | 13.3 | 3.07 |
| 79635 | 1.1 | 0.8 | 6 | 2.5 | 60 | 1.23 | 4.9 | 2.6 |
| 75590 | 1.7 | 1.3 | 10 | 3.1 | 106 | 1.38 | 12.3 | 2.82 |
| 77922 | 2.3 | 1.7 | 17 | 4.77 | 116 | 1.37 | 20.7 | 2.74 |

*Table 1. Parameters of simulated discharges: magnetic field, plasma current, NBI power, line averaged density, toroidal rotation velocity measured at 3m, $H_{98(y,2)}$ factor, plasma pressure at ρ = 0.8 and normalised β. These parameters are averaged over 0.5 s time interval where the highest plasma performance has been obtained.*

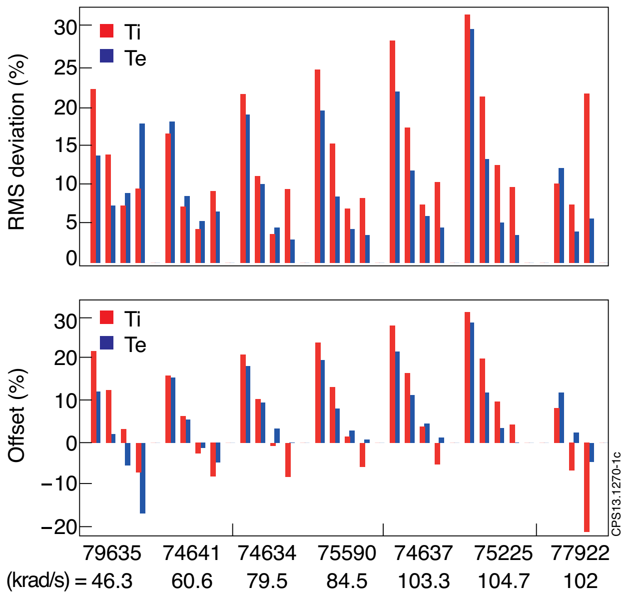


*Figure 1: Rms deviation and offset for electron (blue) and ion (red) temperature estimated with $\alpha_E$ = 0, 0.5, 1 and 1.3 (columns from the left to the right within each group of eight columns) in the low density discharges and with αE = 0, 0.5 and 1 in the medium density discharge Pulse No: 77922. Toroidal angular frequency Ω at ρ = 0.25 averaged over the selected 0.5 s time window is indicated for each discharge. A positive offset means that the temperature profiles are underpredicted in simulations.*

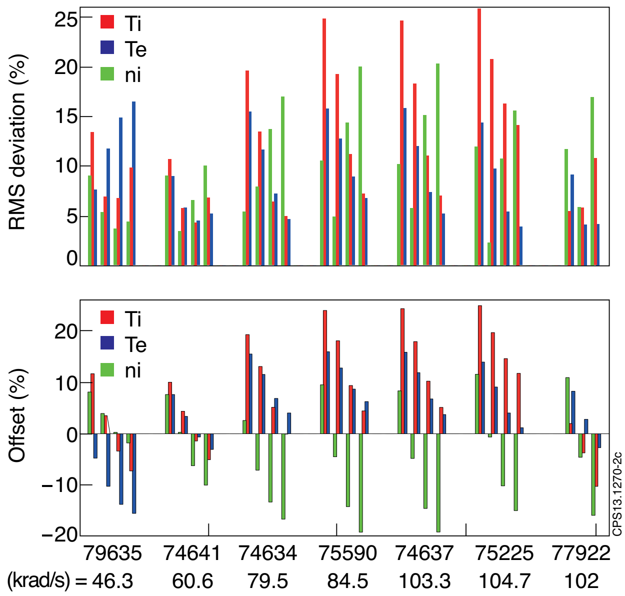


*Figure 2: Rms deviation and offset for $T_e$ (blue), $T_i$ (red) and $n_i$ (green) estimated with $\alpha_E$ = 0, 0.5, 1 and 1.3 in the low density discharges and with $\alpha_E$ = 0, 0.5 and 1 in the medium density discharge Pulse No: 77922.*

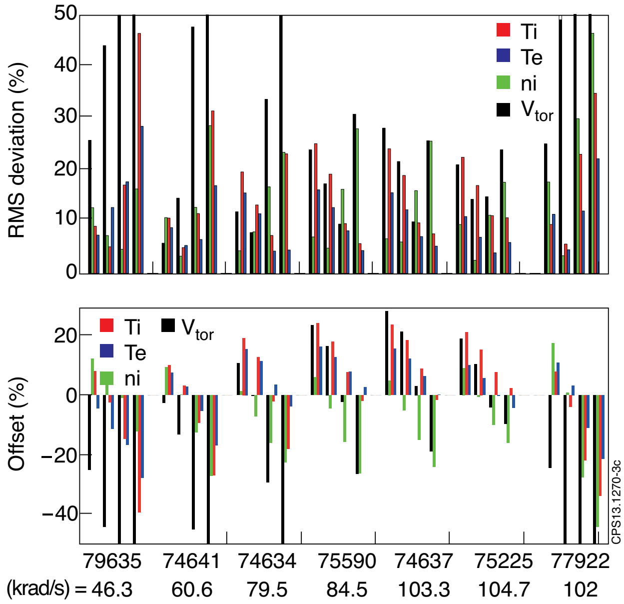


*Figure 3: Rms deviation and offset for $T_e$ (blue), $T_i$ (red), $n_i$ (green) and $V_{tor}$ (black) estimated with $\alpha_E$ = 0, 0.5, 1 and 1.3.*

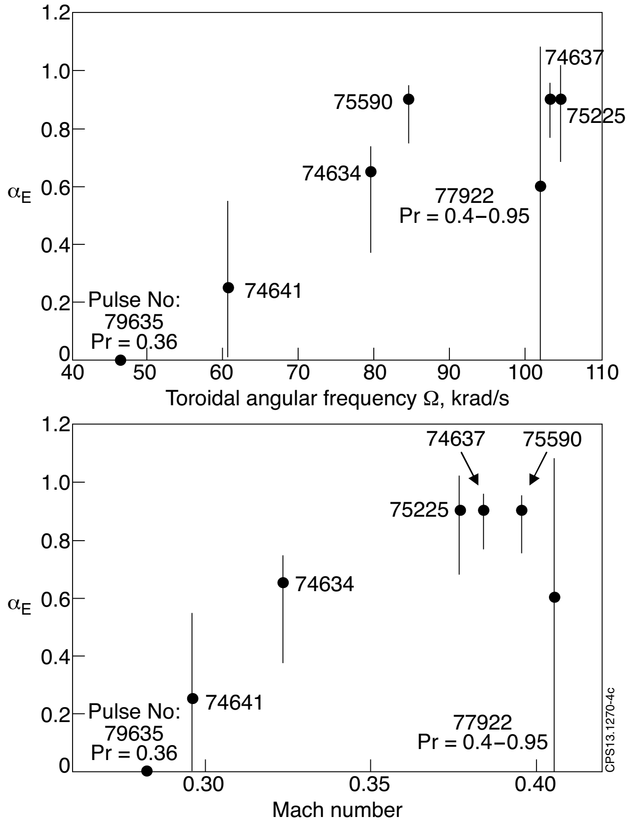


*Figure 4: αE values providing the most accurate prediction of $T_e$, $T_i$, $n_i$ and $V_{tor}$ in each simulated discharge (circles) versus toroidal angular frequency (top) and Mach number (bottom). Vertical lines show the $\alpha_E$ uncertainty limited by 15% deviation between simulated and measured quantities. Pr = 0.3 is used for all discharges except Pulse No's: 79635 (Pr = 0.36) and 77922 (range of Prandtl numbers is shown on Fig.7). Toroidal angular frequency and Mach number are estimated at ρ = 0.25 and averaged over half-second time window.*

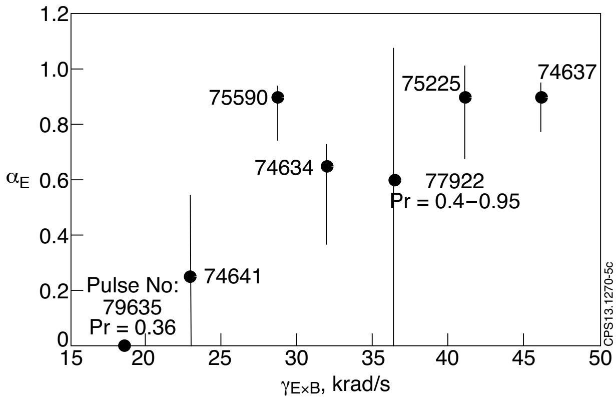


*Figure 5: Same parameters as on Fig.4 plotted as a function of $\gamma_{E\times B}$ averaged over 0.25 ≤ ρ ≤ 0.65 and over the selected half-second time window.*

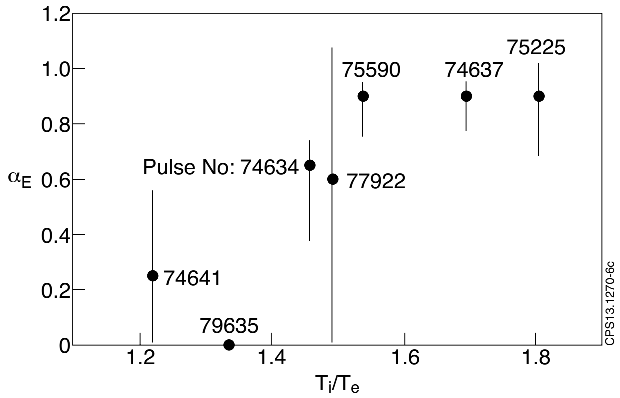


*Figure 6: Same parameters as on Fig.4 plotted as a function of $T_i/T_e$ estimated at ρ = 0.25 and averaged over half-second time window.*

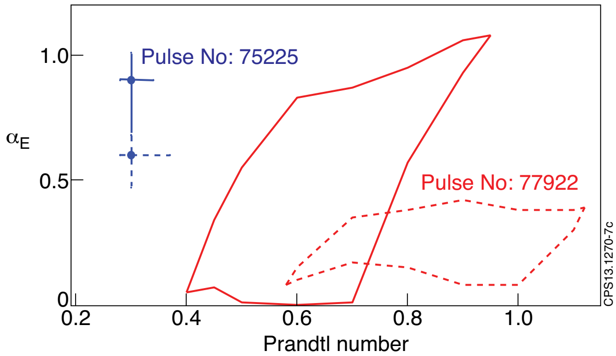


*Figure 7: Pr - $\alpha_E$ domain for Pulse No: 77922 limited by 15% deviation between the electrostatic (red solid curve) and electromagnetic (red dashed curve) GLF23-based prediction of Te, Ti, ni and Vtor and measurements. Prandtl number and $\alpha_E$ uncertainties obtained for discharge Pulse No: 75225 under the same assumption are shown for comparison (solid (dashed) curves correspond to electrostatic (electromagnetic) GLF23 computed transport).*

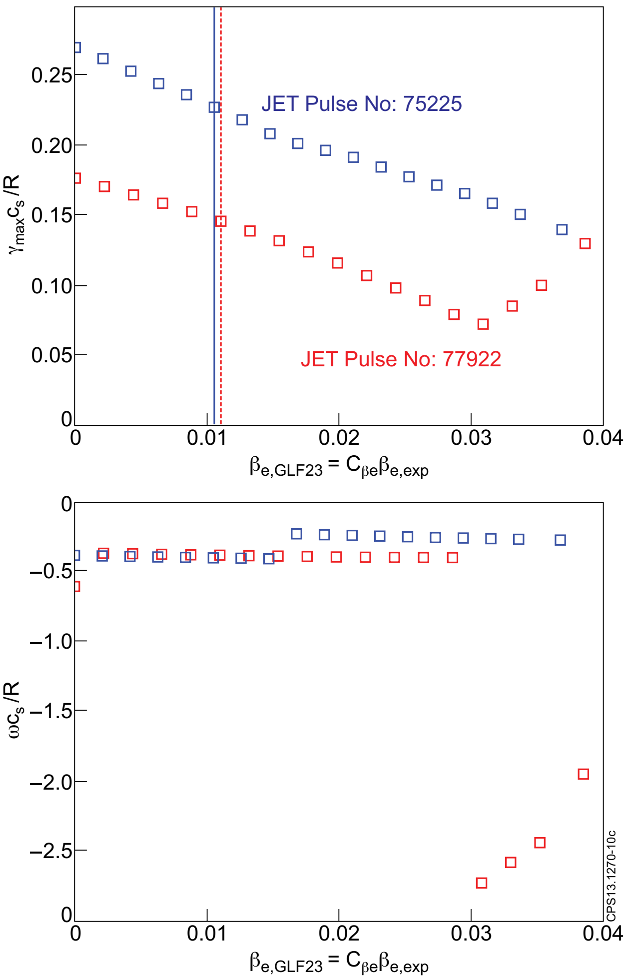


*Figure 8: $\beta_e$ dependence of maximum linear growth rate (top) and corresponding frequency (bottom) at ρ = 0.4 calculated with measured profiles for Pulse No's: 75225 (blue symbols) and 77922 (red symbols). Vertical lines on the top figure indicate the experimental $\beta_e$ values.time window.*

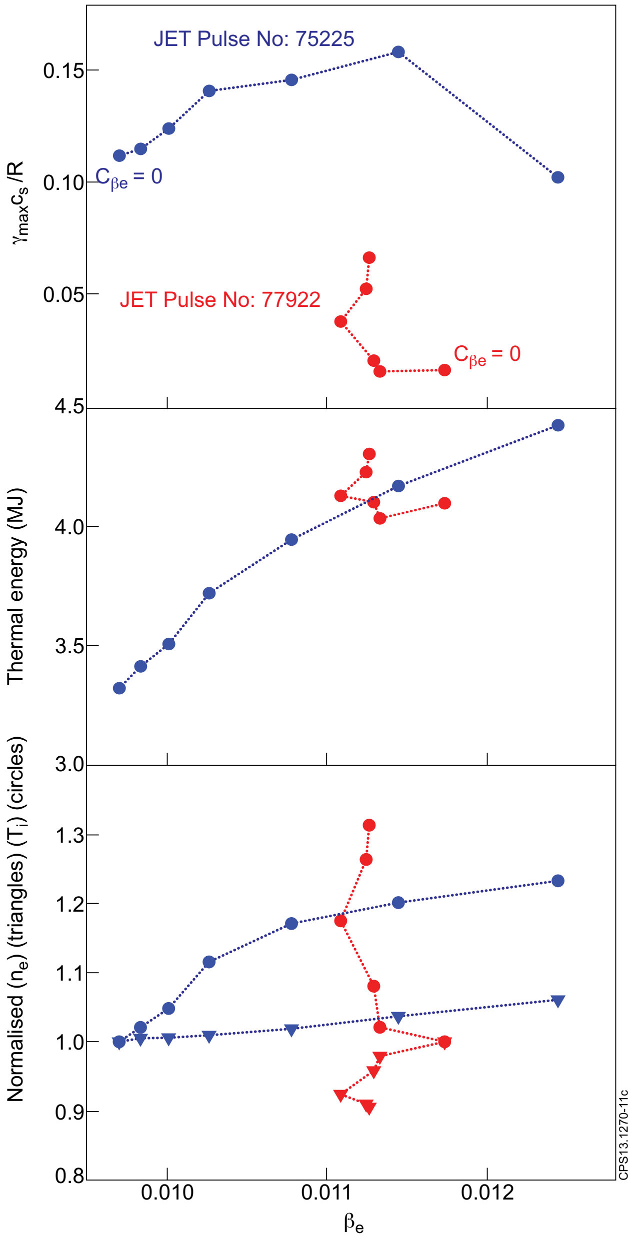


*Figure 9: βe dependence of maximum linear growth rate at ρ = 0.4 (top) and thermal energy (middle) for Pulse No's: 75225 (blue symbols) and 77922 (red symbols) obtained in self-consistent simulations by changing $C\beta_e$. Bottom panel shows the variation of volume averaged electron density $<n_e>$ (triangles) and ion temperature $<T_i>$ (circles) normalised to their values obtained with electrostatic GLF23 model with $\beta_e$.*

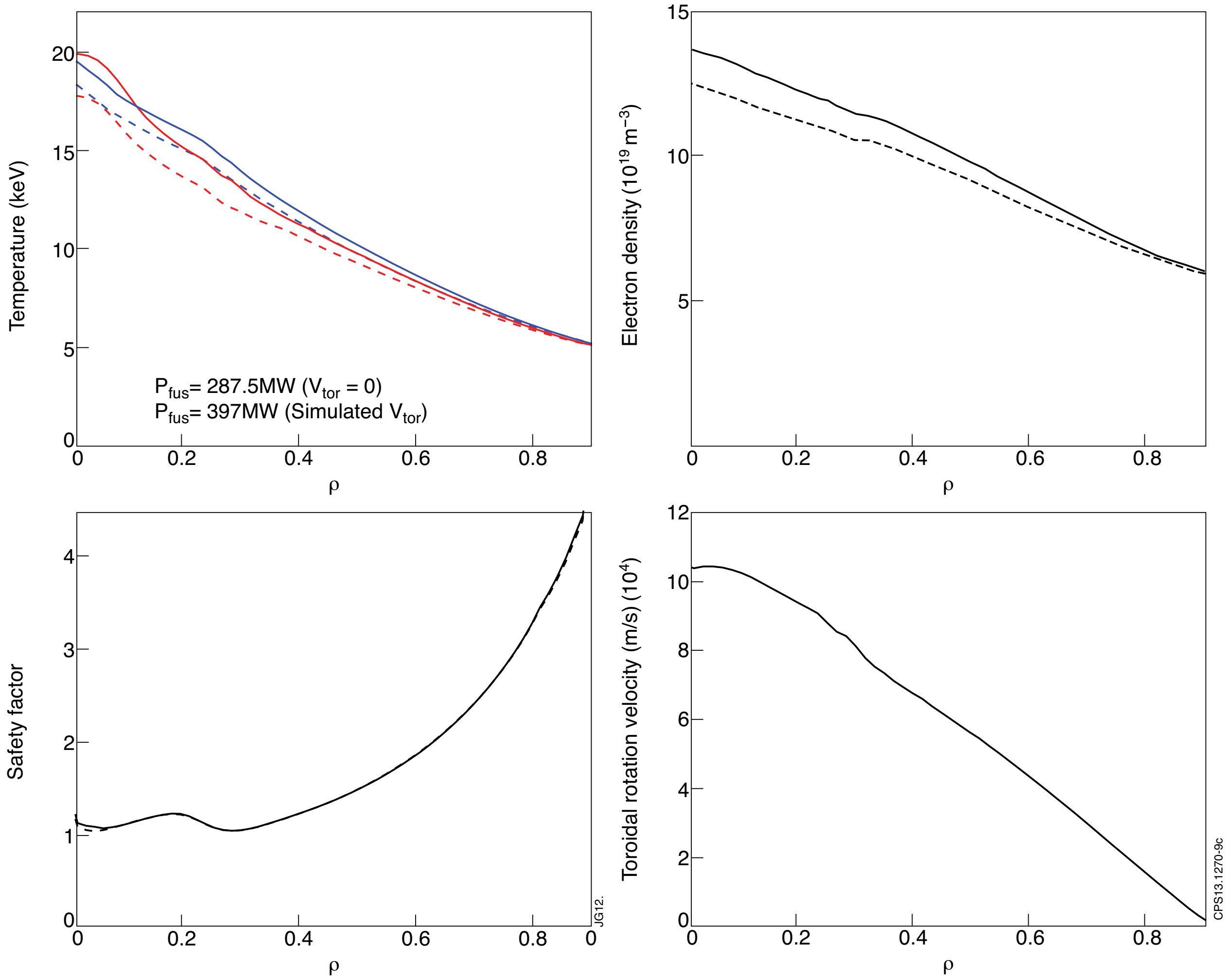


*Figure 10: Electron (blue curves) and ion (red curves) temperature (top left), electron density (top right), q profile (bottom left) and toroidal rotation velocity (bottom right) obtained in ITER hybrid scenario by using Pr = 0.3 and $\alpha_E$ = 0.9 (solid curves). Dashed curves show $T_i$, $T_e$ and $n_e$ obtained with zero toroidal rotation and $\alpha_E$ = 0.5. Fusion power for two cases is indicated in the top left panel.*